

# The Transit Light Curve Project.

## XII. Six Transits of the Exoplanet XO-2b

Jose M. Fernandez<sup>1,2</sup>, Matthew J. Holman<sup>1</sup>, Joshua N. Winn<sup>3</sup>, Guillermo Torres<sup>1</sup>, Avi Shporer<sup>4</sup>, Tsevi Mazeh<sup>4</sup>, Gilbert A. Esquerdo<sup>1</sup>, Mark E. Everett<sup>5</sup>

### ABSTRACT

We present photometry of six transits of the exoplanet XO-2b. By combining the light-curve analysis with theoretical isochrones to determine the stellar properties, we find the planetary radius to be  $0.996^{+0.031}_{-0.018} R_{\text{Jup}}$  and the planetary mass to be  $0.565 \pm 0.054 M_{\text{Jup}}$ . These results are consistent with those reported previously, and are also consistent with theoretical models for gas giant planets. The mid-transit times are accurate to within 1 min and are consistent with a constant period. However, the period we derive differs by  $2.5\sigma$  from the previously published period. More data are needed to tell whether the period is actually variable (as it would be in the presence of an additional body) or if the timing errors have been underestimated.

*Subject headings:* planetary systems—stars: individual (XO-2, GSC 03413-00005)

### 1. Introduction

Observations of exoplanetary transits have provided the first empirical information about the internal structure, composition, surface temperature and atmospheric dynamics of planets outside the Solar system (Charbonneau et al. 2007). It is hoped that precise

---

<sup>1</sup>Harvard-Smithsonian Center for Astrophysics, 60 Garden Street, Cambridge, MA 02138, USA; jfernand@cfa.harvard.edu.

<sup>2</sup>Department of Astronomy, Pontificia Universidad Católica, Casilla 306, Santiago 22, Chile.

<sup>3</sup>Department of Physics, and Kavli Institute for Astrophysics and Space Research, Massachusetts Institute of Technology, Cambridge, MA 02139, USA.

<sup>4</sup>Wise Observatory, Raymond and Beverly Sackler Faculty of Exact Sciences, Tel Aviv University, Tel Aviv 69978, Israel.

<sup>5</sup>Planetary Science Institute, 1700 East Fort Lowell Road, Suite 106, Tucson, AZ 85719, USA.

measurements of transit times and durations will also provide a new channel for the detection of low-mass planets (Holman & Murray 2005; Agol et al. 2005). Among the immense amount of information these systems may deliver, the most fundamental parameter is the radius of the planet. Accurate radius determination is not a trivial task, and in some cases after a transiting planet has been announced, more precise data have led to significant revisions on their radius, with consequences for theories of planetary interiors and atmospheres (see, e.g. Winn et al. 2008; Johnson et al. 2008).

The Transit Light Curve (TLC) project is an effort to gather precise photometry of exoplanetary transits, in order to determine the fundamental properties of these planets and their parent stars as accurately as possible, and to seek evidence of undetected planets in the pattern of transit times and durations.

The present paper is concerned with the XO-2 system (Burke et al. 2007). This was the second system discovered by the XO project (McCullough et al. 2006). The XO-2 star is a nearby Solar-type star with a binary companion (identified through its common proper motion), and has a high metallicity ( $[\text{Fe}/\text{H}] = 0.45$ ) compared to other planet-hosting stars. The XO-2b planet is a normal hot Jupiter (if the word “normal” may be applied to such interesting objects), with an orbital period  $P = 2.615857 d$ , mass  $M = 0.57M_{\text{Jup}}$ , and radius  $R = 0.98R_{\text{Jup}}$  (Burke et al. 2007).

In this work we present and analyze differential photometry of six transits of XO-2b. We measured the mid-transit time for each of the six events, and by combining the data, we obtained new and independent estimates for the system parameters. This paper is organized as follows. In § 2 we describe the observations and data reduction procedure. In § 3 we describe the model and the techniques we used to estimate the physical parameters of this system. In § 4 we present the results for the planetary parameters and mid-transit times. Finally, in § 5 we present a brief summary of this work.

## 2. Observations and Data Reduction

We observed four complete transits, and one partial transit, with the 1.2 m (48-inch) telescope at the Fred L. Whipple Observatory (FLWO) on Mount Hopkins, in Arizona. The FLWO 1.2m telescope is equipped with KeplerCam, a monolithic  $4\text{K} \times 4\text{K}$  Fairchild 486 CCD that gives a  $23' \times 23'$  field and a pixel size of  $0.68''$  in  $2 \times 2$  binned mode. We used a Sloan  $z$  band filter to minimize the effects of limb darkening on the shape of the transit light curve.

We observed one complete transit with the Centurion 0.46 m (18-inch) telescope, at the Wise Observatory, in Israel. The Centurion telescope is equipped with a Santa Barbara

Instrument Group (SBIG) ST-10 XME USB CCD camera. This thermoelectrically-cooled chip has  $2184 \times 1472$  pixels each  $6.8 \mu\text{m}$  wide, which convert to 1.1 arcsec at the  $f/2.8$  focus of the telescope. The chip offers a  $40.5' \times 27.3'$  field of view. Observations from Wise were made with no filter, because this camera has no filter wheel. The 18-inch telescope CCD has an overall response similar to a “wide-R” band (for further details, see Brosch et al. 2008).

Relative aperture photometry was performed for XO-2 and 13 nearby comparison stars, including the binary companion of XO-2 (7 stars were used for the Wise data set). The choice of comparison stars was iterative; we began with a longer list, and those stars that showed unusual noise or variability were removed. The 13 comparison stars range in brightness from 50–200% of the brightness of XO-2. The sum of the fluxes of the comparison stars was taken to be the reference signal, and the flux of XO-2 was divided by this reference signal. The root-mean-square (rms) noise in the relative flux of XO-2 among the six light curves ranges between 0.0013 and 0.0036. Table 1 gives a summary of the six photometric observations, with information about the dates, epochs, band, exposure times and RMS. Figure 1 shows the observed light curves. A differential airmass correction was applied to the plotted light curves. This correction was determined as part of the fitting process that is described in the next section. Table 2 has an abbreviated versions of one of the light curves. We intend for the complete photometric data set to appear in the electronic version of the journal.

### 3. Data Modeling

#### 3.1. Light Curve Analysis

We modeled the light curves using the analytic formulas of Mandel & Agol (2002). The orbital period was held fixed using the value of Burke et al. (2007) and the planetary orbit was assumed to be circular. The fitted parameters were the radius ratio  $R_p/R_\star$ , the normalized semi-major axis  $a/R_\star$ , the impact parameter  $b$ , the mid-transit time  $T_c$ , and two parameters that take into account the zero-point and slope of the differential airmass correction. We assumed a quadratic limb-darkening law, with coefficients  $u_1$  and  $u_2$ . Through a trial fit, we found that the data are not precise enough to fit for both limb-darkening coefficients. The linear combination  $2u_1 + u_2$  is well-constrained, and the orthogonal combination  $u_1 - 2u_2$  is poorly constrained. For this reason we allowed  $2u_1 + u_2$  to be a free parameter, and held  $u_1 - 2u_2$  fixed. We fixed  $u_1 - 2u_2$  at the value tabulated by Claret (2004)<sup>1</sup>, for a star with the metallicity, gravity, and temperature derived by Burke et al. (2007).

---

<sup>1</sup>From Claret (2004),  $u_1 = 0.292$  and  $u_2 = 0.299$

The fitting statistic was

$$\chi_{lc}^2 = \sum_{j=1}^{N_f} \left[ \frac{f_j^{obs} - f_j^{mod}}{\sigma_j} \right]^2 \quad (1)$$

where  $f_j^{obs}$  and  $f_j^{mod}$  are the observed and modeled relative fluxes observed at time  $j$ , and  $\sigma_j$  is the uncertainty of the data points as described below. To set the appropriate data weights, we used a procedure that attempts to account for any time-correlated (“red”) noise, at least approximately. For each light curve we found an initial best-fitting model (using the out-of-transit RMS as the flux weight) and calculated  $\sigma_1$ , the standard deviation of the unbinned residuals between the observed and calculated fluxes. Next we averaged the residuals into  $M$  bins of  $N$  points and calculated the standard deviation of the binned residuals. In the absence of red noise, we would have expected

$$\sigma_N = \frac{\sigma_1}{\sqrt{N}} \sqrt{\frac{M}{M-1}} \quad (2)$$

but often the measured value of  $\sigma_N$  is larger than this by a factor  $\beta$  due to time-correlated noise. In such cases the number of effectively independent data points is smaller than the actual number of data points. In Eq. 1 we used  $\sigma_j = \sigma_1 \times \beta$ . We found that  $\beta$  depends weakly on the choice of averaging time  $\tau$ , generally rising to an asymptotic value at  $\tau \sim 10$  minutes. The value  $\beta$  was close to unity except for the light curves of UT 2008 Feb 25 ( $\beta = 1.2$ ) and UT 2008 Mar 06 ( $\beta = 1.5$ ).

The best-fit parameters and their uncertainties were obtained using a Markov Chain Monte Carlo (MCMC) procedure. As described by Ford (2005) and Holman et al. (2006), in this method a random process is used to create a sequence of points in the parameter space that approximates the studied probability distribution. This sequence or chain is generated by a jump function that adds a Gaussian random number to each parameter. The jump is executed if the new point has a  $\chi_{lc}^2$  lower than the previous point. If  $\chi_{lc}^2$  is larger, the jump is made with a probability equal to  $\exp(-\Delta\chi_{lc}^2/2)$ . If the jump is not made, the new point is a copy of the previous one. The relative sizes of the perturbation were set equal to the approximate  $1\sigma$  uncertainties obtained by direct inspection of  $\chi_{lc}^2$  across the parameter space, as done in Beatty et al. (2007). The sizes of the jumps are set by requiring that  $\sim 25\%$  of the jumps are accepted. As a first step, four independent chains of  $2 \times 10^5$  points were created for each light-curve, discarding the first 20 % of points to minimize transient effects. The four chains were then superposed to create one sequence of points. The Gelman & Rubin (1992) R statistic was always within 0.2% of unity for each parameter, a sign of good mixing and convergence. The cumulative posterior probability is a normalized histogram of the MCMC sample values. To derive the confidence interval for a parameter, the MCMC sets were sorted by the parameter of interest and then we determined the 15.85%, 50%, and

84.15% points of the cumulative posterior distribution. The 50% point (i.e. the median) was taken to be the “best-fitting value” and the interval between the 15.85% and 84.15% points was taken to be the 68.3% ( $1-\sigma$ ) confidence interval.

The final values for the transit parameters  $R_p/R_\star$ ,  $a/R_\star$  and  $b$  were obtained by analyzing the combined data from the five light curves observed with FLWO/KeplerCam, following the same procedure used for the individual transits. A 2-minute binned version of these combined light curves is shown in Figure 2.

For the transit timings, we also performed two independent additional tests to check the accuracy of our results. For one of the tests we used a standard bootstrap simulation: we created  $10^4$  “realizations” of the data set by perturbing the best-fitting model with Gaussian random noise (with a standard deviation equal to the rms of the actual light curve), and minimizing  $\chi_{i_c}^2$  as a function of  $t_c$  for each realization ( $R_p/R_\star$ ,  $a/R_\star$  and  $b$  are not correlated with  $t_c$ , and were therefore held fixed for these tests). The resulting collection of  $10^4$  timings for each transit was taken to be the probability distribution of the timing (see, e.g., Press et al. 1992). For the second test we implemented the residual-permutation or “rosary-bead” method. For each light curve, we found the best-fitting model and computed the time series of  $N$  residuals. We then added these residuals to the model light curve after performing a cyclic permutation of the time indices. This is a variant of the bootstrap technique that preserves the temporal correlations among the residuals, and has been used previously by many investigators (e.g., Bouchy et al. 2005; Southworth 2008). For the six light curves under study, the timings obtained on the additional tests were consistent with our first set of results, and with similar error bars. The results of the light curve analysis are summarized in Table 3.

### 3.2. Determination of Absolute Dimensions

As has been shown before by several authors, the only intrinsic properties of the star and planet that can be determined directly from observed quantities on transiting systems are the mean density of the star (Seager & Mallén-Ornelas 2003) and the surface gravity of the planet (Sozzetti et al. 2007; Holman et al. 2007; Southworth et al. 2004). In order to determine the individual masses and radii of the bodies, external information must be introduced.

In this case, we used stellar evolution models following the procedure and considerations of Torres et al. (2008). For this purpose we rely on the spectroscopic temperature ( $T_{\text{eff}} = 5340 \text{ K}$ ) and metallicity ( $[\text{Fe}/\text{H}] = 0.45$ ) obtained by Burke et al. (2007),

but we adopt more conservative errors, no smaller than 0.05 dex in  $[\text{Fe}/\text{H}]$  and 80 K in  $T_{\text{eff}}$ . The reason for this approach is to take into account the documented difficulty in obtaining accurate values for stellar temperatures (see, eg., Blackwell & Shallis 1977; Blackwell et al. 1980; Casagrande et al. 2006; Ramírez & Meléndez 2005) and metallicities (see, eg., Fischer & Valenti 2005; Gonzalez & Laws 2007; Santos et al. 2004). Instead of using the spectroscopic value for  $\log g$ , we used the parameter  $a/R_{\star}$  that is closely related to the mean stellar density and it is provided by the transit light curve fit. The quantity  $a/R_{\star}$  can be obtained from the models using the following expression:

$$a/R_{\star} = \left( \frac{G}{4\pi^2} \right)^{1/3} \frac{P^{2/3}}{R_{\star}} (M_{\star} + M_p)^{1/3}. \quad (3)$$

The mass of the planet is not known a priori, but  $a/R_{\star}$  can be estimated using the value of  $M_p$  derived by Burke et al. (2007). At the end of the procedure to be explained next, a new value of  $M_p$  is obtained, which is used to repeat the process until convergence.

The stellar evolution models used were those from the Yonsei-Yale series (Yi et al. 2001; Demarque et al. 2004). These isochrones were interpolated to a fine grid in metallicity and age and compared point by point with the measured values of  $T_{\text{eff}}$  and  $a/R_{\star}$ . Each point on the isochrones that was consistent with  $[\text{Fe}/\text{H}]$ ,  $T_{\text{eff}}$  and  $a/R_{\star}$  within their errors, was recorded and a likelihood given by  $\exp(-\chi_{\star}^2/2)$  was calculated, where

$$\chi_{\star}^2 = \left( \frac{\Delta [\text{Fe}/\text{H}]}{\sigma_{[\text{Fe}/\text{H}]}} \right)^2 + \left( \frac{\Delta T_{\text{eff}}}{\sigma_{T_{\text{eff}}}} \right)^2 + \left( \frac{\Delta (a/R_{\star})}{\sigma_{a/R_{\star}}} \right)^2 \quad (4)$$

In this expression the  $\Delta$  symbols represent the difference between the observed and model values for each quantity. The best fit value for each stellar parameter was obtained by adding all matches, weighted by their corresponding normalized likelihood. We did not account for the varying density of stars on each isochrone, as the effect is generally small in the case of solar-type stars. The adopted errors for the fitted parameters (mass and age) come from their range among the accepted points on the isochrones. Figure 3 illustrates the location of the star in a diagram of  $a/R_{\star}$  vs. effective temperature, similar to an H-R diagram, compared with isochrones from the Yale-Yonsei series.

With  $M_{\star}$  known, we obtained  $M_p$  and  $a$  by iteration of Newton’s modified version of Kepler’s third law and the mass function of the system:

$$a^3 = \frac{G}{4\pi^2} (M_{\star} + M_p) P^2 \quad (5)$$

$$M_p = \left( \frac{P}{2\pi G} \right)^{1/3} \frac{K_{\star}}{\sin i} (M_{\star} + M_p)^{2/3} \quad (6)$$

The value of  $a$  in combination with  $a/R_\star$  and  $R_p/R_\star$  allowed us to obtain consistent values for  $R_\star$  and  $R_p$ .

To estimate the errors for  $M_p$ ,  $R_\star$  and  $R_p$ , we used the MCMC chains generated in the course of modeling the transiting light curves. For each element of the chain a solution was calculated using random Gaussian values for  $P$  and  $K_\star$  (using the observed values and their uncertainties as the center and standard deviation of the Gaussian distributions). In this way we obtained a probability distribution for  $M_p$ ,  $R_\star$ , and  $R_p$ , from which we extracted the median and 68.3% confidence intervals and adopted them as best values and errors, respectively.

It is important to note that our procedure places complete trust in the Yonsei-Yale isochrones. It assumes they are exactly correct. Any systematic errors in the isochrones are not accounted for in our error bars. As this star is very similar to the Sun, we expect these errors to be small.

## 4. Results

Table 3 gives all the measured planetary and stellar properties, together with the results for the light-curve parameters. The labels, explained in the caption, clarify which quantities were obtained from the literature, which were determined independently by our analysis, which quantities are functions of those independent parameters, and which quantities depend on our stellar isochrone analysis.

### 4.1. Planetary and stellar Properties

The light curve best-fit parameters  $a/R_\star$ ,  $R_p/R_\star$  and  $b$  presented in this work are consistent with those obtained by Burke et al. (2007) in the discovery paper of XO-2b, with similar error bars for all of them. The precision of these parameters is dominated by the first and third light curves, which have the highest signal-to-noise ratio. For our stellar isochrone analysis, we used the values for  $T_{\text{eff}}$  and  $[\text{Fe}/\text{H}]$  from the discovery paper about XO-2b, together with our value for  $a/R_\star$ . We obtained a stellar mass value ( $M_\star = 0.971 \pm 0.043$ ) almost identical to the one found by Burke et al. (2007). In our case, the result does not depend on the assumed distance to the star, but only on  $T_{\text{eff}}$  and  $[\text{Fe}/\text{H}]$ . We derived the planetary mass and radius plus the stellar radius directly from the stellar mass. None of these parameters show any significant discrepancy from those listed in the discovery paper. Our error bars are similar as well, but in this work we took into account the red noise in the light

curves and adopted larger errors for  $T_{\text{eff}}$  and  $[\text{Fe}/\text{H}]$ , and in this sense our error estimates are more conservative. In the case of the stellar radius  $R_{\star}$ , the value obtained directly from the isochrone modeling and the one derived from the stellar mass are identical, but the error bars on the latter are 25% smaller. Our stellar surface gravity estimate ( $\log g_{\star} = 4.45 \pm 0.01$ ) is independent from the one obtained by Burke et al. (2007). Both estimates of the surface gravity are in agreement, and our result based on  $a/R_{\star}$  is more precise. This illustrates the power of transit light curves to pin down the stellar mean density, as also exhibited for the XO-3 system (Winn et al. 2008).

As mentioned earlier, we determined the stellar properties following the procedure and considerations of Torres et al. (2008), therefore, we expected our results for XO-2b to be in good agreement with theirs. This is actually the case, given that our analysis of the transit light curves didn't deliver parameters significantly different to the ones obtained by Burke et al. (2007).

We found that the mass and radius for XO-2b are in good agreement with those predicted by Fortney et al. (2007) for a planet orbiting a solar-like star. Interpolation of the tabulated results presented on their work for the appropriate values of the XO-2 system ( $M_p = 0.57M_{\text{Jup}}$ ,  $a = 0.037 \text{ AU}$ ) gives a theoretical planetary radius of  $1.0R_{\text{Jup}}$ .

## 4.2. Transit Timings

Using our 6 transit times, we computed an ephemeris independent of that of Burke et al. (2007), by fitting a linear function of transit epoch  $E$ ,

$$T_c(E) = T_0 + EP. \quad (7)$$

The result is  $T_0 = 2,454,466.88514 \pm 0.00019$  [HJD] and  $P = 2.615819 \pm 0.000014$  days. The fit has  $\chi^2 = 5.76$  with 4 degrees of freedom ( $N_{\text{dof}} = 4$ ), indicating an acceptable fit (i.e.  $\chi^2$  is within  $\sqrt{2N_{\text{dof}}}$  of  $N_{\text{dof}}$ ). However, the fitted period differs by  $2.5\sigma$  (3.3 s) from the value  $2.615857 \pm 0.000005$  d that was determined by Burke et al. (2007).

It is not clear how to interpret this discrepancy. It may be a genuine period variation produced by an additional body in the XO-2 system. However it seems at least as likely that the uncertainties in one or a few of the transit times have been underestimated. Our methods and cross-checks on the errors have already been described. As for Burke et al. (2007), one of their mid-transit times was based on observations with a 1.8m telescope, and has a quoted precision that is better than any of our 6 measurements ( $2,454,147.74902 \pm 0.00020$ ). The other 11 light curves came from observations with smaller telescopes. For those 11, Burke et al. (2007) estimated an error of 3 min, based on the scatter among 3 independent

measurements of one particular transit in March 2007. The relative quality of the individual light curves, which were gathered by different observers on different nights, was not taken into account.

One might wonder if the discrepancy can be attributed to any particular data point. If we use only the most precise time of Burke et al. (2007) in combination with our 6 times, fitting a linear ephemeris gives  $\chi^2 = 15.9$  and  $N_{\text{dof}} = 5$ , which is still unacceptable. If we omit the most precise time and instead use the other 11 times from Burke et al. (2007), adopting 3 min errors as they did, we find  $\chi^2 = 20.9$  and  $N_{\text{dof}} = 15$ , right on the margin of acceptability. If we use all of the times from Burke et al. (2007) and omit our last 2 times, which were derived from the noisiest light curves, we find  $\chi^2 = 15.6$  and  $N_{\text{dof}} = 14$ , a satisfactory fit. (Omitting either of our last two times individually does not result in a satisfactory fit.) No further conclusions can be drawn until more times have been measured, over a longer time baseline.

For planning purposes, we recomputed the ephemeris based on all the available transit times (6 from this work, and 12 from Burke et al. 2007). The result is  $T_0 = 2,454,466.88467 \pm 0.00013$  [HJD] and  $P = 2.6158640 \pm 0.0000016$  d, with  $\chi^2 = 27.6$  and  $N_{\text{dof}} = 16$ . Observers who are using these values to plan future observations may wish to inflate the error bars by  $\sqrt{\chi^2/N_{\text{dof}}} = 1.31$  to account for possible systematic effects due to either genuine period variations or underestimated measurement errors.

A more detailed study of possible short-term transiting timing variations caused by additional orbiting bodies would require the observation of a larger number of consecutive transits, as noted by Holman & Murray (2005) and tested by Miller-Ricci et al. (2008). Any constraint derived from the present data would be of limited interest and beyond of the scope of this paper.

## 5. Summary

We have presented new photometric observations of six transits of the exoplanet XO-2b. The analysis of the data independently confirms the previously calculated properties of this planet, leaving little doubt about the orbit and geometric properties of the XO-2 system. We found that the mass and radius for XO-2b are in good agreement with standard models of gas giant planets. The six new transit timings yield a refined transit ephemeris and set an updated and precise reference for future searches of secondary bodies orbiting this star.

This work was partly supported by NASA Origins Grant No. NNX09AB33G, and by Grant No. 2006234 from the United States-Israel Binational Science Foundation (BSF). KeplerCam was developed with partial support from the Kepler Mission under NASA Cooperative Agreement NCC2-1390 and the KeplerCam observations described in this paper were partly supported by grants from the Kepler Mission to SAO and PSI.

## REFERENCES

- Agol, E., Steffen, J., Sari, R., & Clarkson, W. 2005, *MNRAS*, 359, 567
- Beatty, T. G., Fernández, J. M., Latham, D. W., Bakos, G. Á., Kovács, G., Noyes, R. W., Stefanik, R. P., Torres, G., Everett, M. E., & Hergenrother, C. W. 2007, *ApJ*, 663, 573
- Blackwell, D. E., Petford, A. D., & Shallis, M. J. 1980, *A&A*, 82, 249
- Blackwell, D. E., & Shallis, M. J. 1977, *MNRAS*, 180, 177
- Bouchy, F., Pont, F., Melo, C., Santos, N. C., Mayor, M., Queloz, D., & Udry, S. 2005, *A&A*, 431, 1105
- Brosch, N., Polishook, D., Shporer, A., Kaspi, S., Berwald, A., & Manulis, I. 2008, *Ap&SS*, 314, 163
- Burke, C. J., McCullough, P. R., Valenti, J. A., Johns-Krull, C. M., Janes, K. A., Heasley, J. N., Summers, F. J., Stys, J. E., Bissinger, R., Fleenor, M. L., Foote, C. N., García-Melendo, E., Gary, B. L., Howell, P. J., Mallia, F., Masi, G., Taylor, B., & Vanmunster, T. 2007, *ApJ*, 671, 2115
- Casagrande, L., Portinari, L., & Flynn, C. 2006, *MNRAS*, 373, 13
- Charbonneau, D., Brown, T. M., Burrows, A., & Laughlin, G. 2007, in *Protostars and Planets V*, ed. B. Reipurth, D. Jewitt, & K. Keil, 701–716
- Claret, A. 2004, *A&A*, 428, 1001
- Demarque, P., Woo, J.-H., Kim, Y.-C., & Yi, S. K. 2004, *ApJS*, 155, 667
- Fischer, D. A., & Valenti, J. 2005, *ApJ*, 622, 1102
- Ford, E. B. 2005, *AJ*, 129, 1706

- Fortney, J. J., Marley, M. S., & Barnes, J. W. 2007, *ApJ*, 659, 1661
- Gonzalez, G., & Laws, C. 2007, *MNRAS*, 378, 1141
- Holman, M. J., & Murray, N. W. 2005, *Science*, 307, 1288
- Holman, M. J., Winn, J. N., Latham, D. W., O’Donovan, F. T., Charbonneau, D., Bakos, G. A., Esquerdo, G. A., Hergenrother, C., Everett, M. E., & Pál, A. 2006, *ApJ*, 652, 1715
- Holman, M. J., Winn, J. N., Latham, D. W., O’Donovan, F. T., Charbonneau, D., Torres, G., Sozzetti, A., Fernandez, J., & Everett, M. E. 2007, *ApJ*, 664, 1185
- Johnson, J. A., Winn, J. N., Cabrera, N. E., & Carter, J. A. 2008, ArXiv e-prints
- Mandel, K., & Agol, E. 2002, *ApJ*, 580, L171
- McCullough, P. R., Stys, J. E., Valenti, J. A., Johns-Krull, C. M., Janes, K. A., Heasley, J. N., Bye, B. A., Dodd, C., Fleming, S. W., Pinnick, A., Bissinger, R., Gary, B. L., Howell, P. J., & Vanmunster, T. 2006, *ApJ*, 648, 1228
- Miller-Ricci, E., Rowe, J. F., Sasselov, D., Matthews, J. M., Kuschnig, R., Croll, B., Guenther, D. B., Moffat, A. F. J., Rucinski, S. M., Walker, G. A. H., & Weiss, W. W. 2008, *ApJ*, 682, 593
- Press, W. H., Teukolsky, S. A., Vetterling, W. T., & Flannery, B. P. 1992, *Numerical recipes in FORTRAN. The art of scientific computing* (Cambridge: University Press, —c1992, 2nd ed.)
- Ramírez, I., & Meléndez, J. 2005, *ApJ*, 626, 465
- Santos, N. C., Israelian, G., & Mayor, M. 2004, *A&A*, 415, 1153
- Seager, S., & Mallén-Ornelas, G. 2003, *ApJ*, 585, 1038
- Southworth, J. 2008, *MNRAS*, 386, 1644
- Southworth, J., Zucker, S., Maxted, P. F. L., & Smalley, B. 2004, *MNRAS*, 355, 986
- Sozzetti, A., Torres, G., Charbonneau, D., Latham, D. W., Holman, M. J., Winn, J. N., Laird, J. B., & O’Donovan, F. T. 2007, *ApJ*, 664, 1190
- Torres, G., Winn, J. N., & Holman, M. J. 2008, *ApJ*, 677, 1324

Winn, J. N., Holman, M. J., Torres, G., McCullough, P., Johns-Krull, C., Latham, D. W., Shporer, A., Mazeh, T., Garcia-Melendo, E., Foote, C., Esquerdo, G., & Everett, M. 2008, *ApJ*, 683, 1076

Yi, S., Demarque, P., Kim, Y.-C., Lee, Y.-W., Ree, C. H., Lejeune, T., & Barnes, S. 2001, *ApJS*, 136, 417

Table 1. PHOTOMETRIC OBSERVATIONS SUMMARY

UT Date	Jan 01 2008	Jan 14 2008	Feb 12 2008	Feb 25 2008	Mar 04 2008	Mar 06 2008
Epoch <sup>1</sup>	0	5	16	21	24	25
Observatory	FLWO	FLWO	FLWO	FLWO	FLWO	Wise
Band	Sloan <i>z</i>	clear				
Exposure [sec]	30	25	25	30	25	9
FWHM <sub>median</sub> [arcsec]	1.6	1.5	1.2	1.4	2.9	1.3
RMS [rel. flux]	0.0013	0.0013	0.0017	0.0027	0.0026	0.0036

Note. — (1)Number of cycles elapsed since the initial transit studied in this work

Table 2. TRANSIT LIGHT CURVE

Jan 01 2008 UT	
HJD	Relative Flux
2454466.78551	0.99807
2454466.78602	1.00079
2454466.78654	1.00180
2454466.78705	0.99955

Note. — This is a sample entry of a full light curve. The complete versions are given on-line.

Table 3. TRANSIT TIMINGS AND SYSTEM PARAMETERS FOR XO-2

Parameter		Value	68.3% Conf. Limits	Comment
$T_c$ (0)	[HJD]	2,454,466.88512	0.00021	A
$T_c$ (5)	[HJD]	2,454,479.96393	0.00039	A
$T_c$ (16)	[HJD]	2,454,508.73864	0.00026	A
$T_c$ (21)	[HJD]	2,454,521.81778	0.00072	A
$T_c$ (24)	[HJD]	2,454,529.66433	0.00043	A
$T_c$ (25)	[HJD]	2,454,532.27978	0.00074	A
$P$	[days]	2.6158640	0.0000016	B
$T_0$	[HJD]	2,454,466.88467	0.00012	B
$R_p/R_\star$		0.10485	+0.00070, -0.00062	A
$a/R_\star$		8.13	+0.09, -0.20	A
$b$		0.16	0.11	A
$u_1$		0.250	0.026	A
$u_2$		0.296	0.013	A
$\rho_{star}$	[ $g\ cm^{-3}$ ]	1.484	+0.051, -0.104	C
$\log g_p$	[ $cm\ s^{-2}$ ]	3.147	+0.043, -0.048	C
$M_\star$	[ $M_\odot$ ]	0.971	0.034	D
$age_\star$	[Gyr]	6.3	2.4	D
$R_\star$	[ $R_\odot$ ]	0.976	+0.024, -0.016	E
$\log g_\star$	[ $cm\ seg^{-2}$ ]	4.448	+0.011, -0.021	E
$M_p$	[ $M_{Jup}$ ]	0.565	0.054	E
$R_p$	[ $R_{Jup}$ ]	0.996	+0.031, -0.018	E
$a$	[AU]	0.0368	0.0004	E

Note. — (A) obtained independently. (B) derived using transit timings from this work and from Burke et al. (2007). (C) calculated using  $K_*$  from Burke et al. (2007). (D) derived from isochrone modeling using values for  $T_{\text{eff}}$  and  $[\text{Fe}/\text{H}]$  from Burke et al. (2007). (E) function of A, C and D

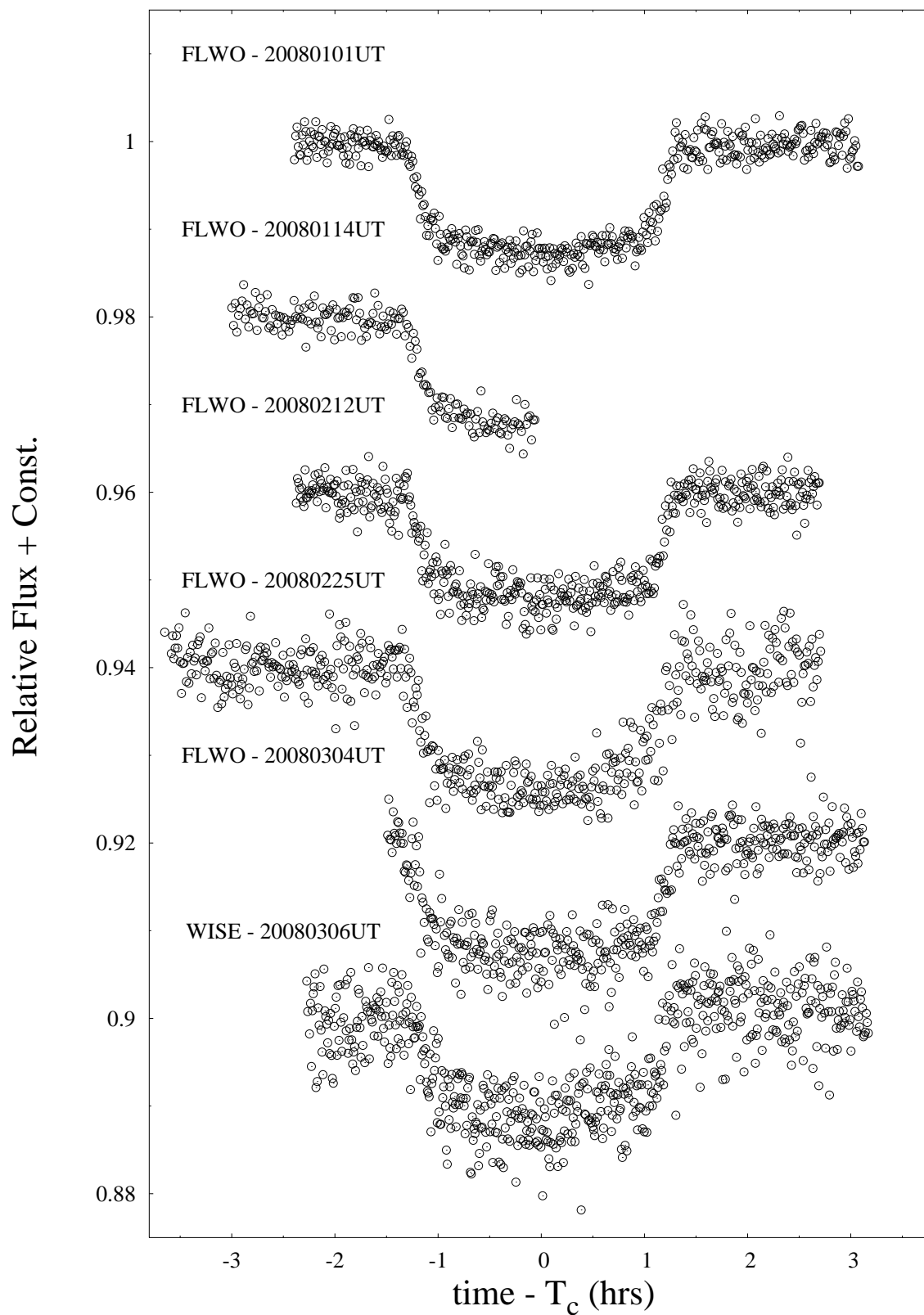


Fig. 1.— Individual transit light curves, after applying a correction for differential extinction. The FLWO transits were observed in the Sloan  $z$  band. No filter was used at Wise; the effective bandpass resembles wide  $R$  band.

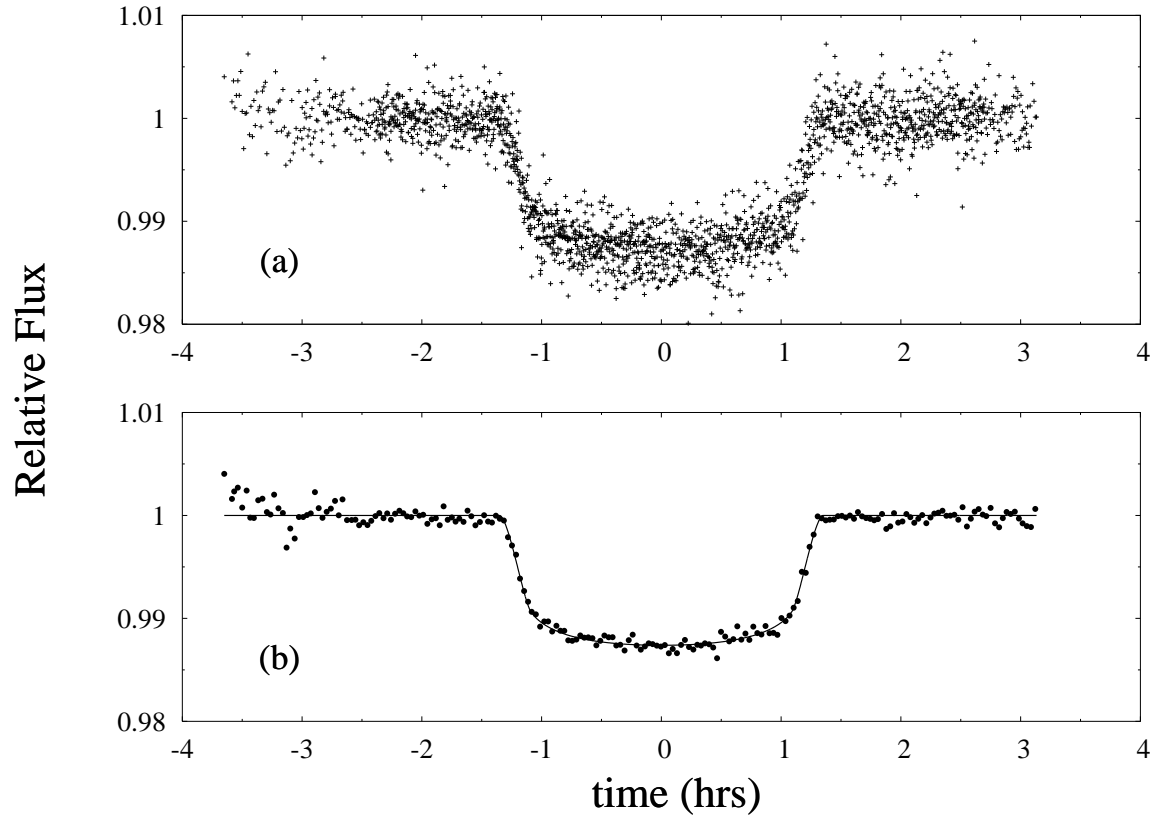


Fig. 2.— A. Combined FLWO light curves. B. Best-fit model and 2 min binned combined light curve. The light curve observed from Wise is not included in this combined data set.

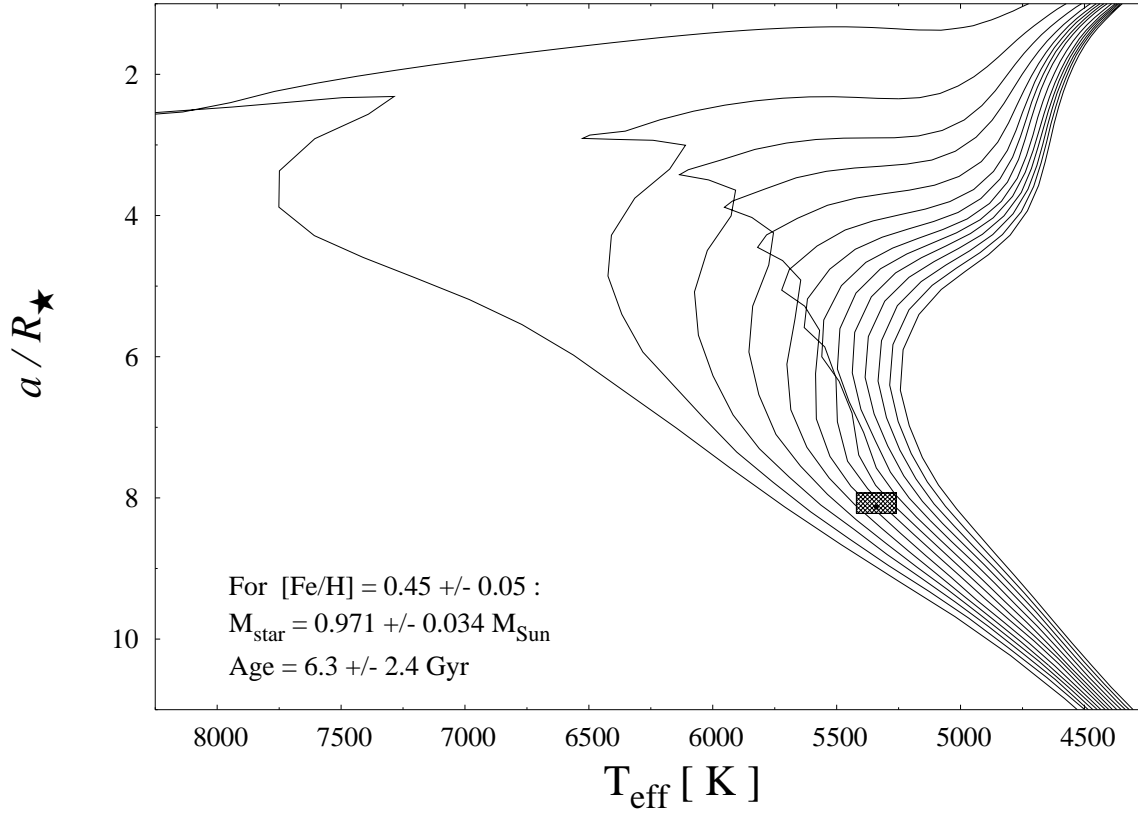


Fig. 3.— Yonsei-Yale stellar isochrones for the modeling of the primary star, corresponding to ages of 0.6 Gyr, 1.6 Gyr, 2.6 Gyr, etc. (left to right), and the chemical composition indicated. The observed transit parameter  $a/R_{\star}$ , which is closely related to the mean stellar density, was used as an indicator of luminosity. The black dot and the filled box around it indicate the best values and uncertainties for  $a/R_{\star}$  and  $T_{\text{eff}}$ .

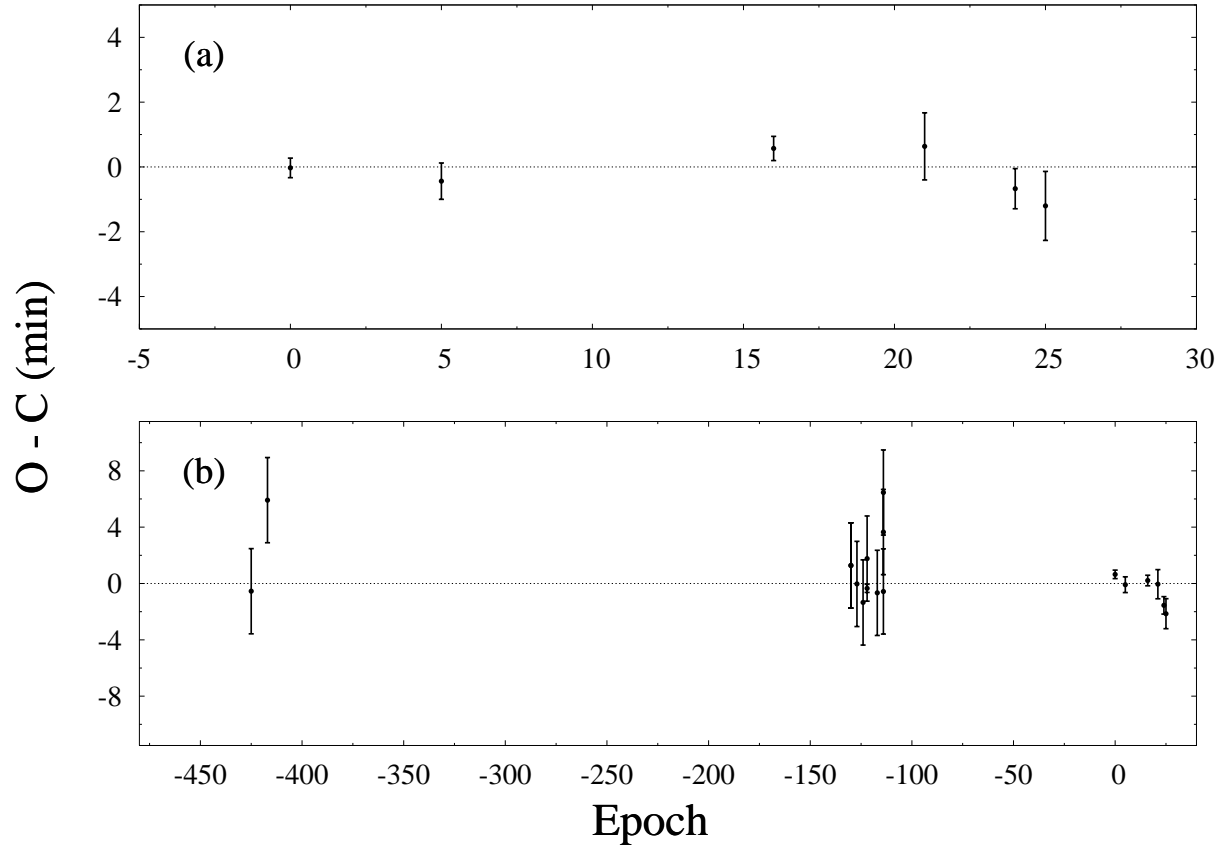


Fig. 4.— Differences between observed and calculated transit times. On panel (a), the 6 TLC transit timings are shown. The time residuals are calculated from the ephemeris obtained using TLC transits only. Panel (b) shows the time residuals of all the transits reported on the discovery paper plus those presented in this work. The time residuals are calculated from the ephemeris obtained using all the available timings.